ANALYTICAL MODEL OF A NEW INTEGRATED COLLECTOR STORAGE SYSTEM HEATED AT THE BOTTOM WITH A STRATIFIER

Jeronimo V. D. Souza[1] and Gilles Fraisse[1]

[1] Locie, UMR-5271, Université de Savoie, Bourget du Lac (France)

1. Introduction

In the context of the French national plan for building energy renovation, we developed a new domestic hot water integrated collector storage (ICS) unit. In order to evaluate the annual performance of this specific bottom-heated ICS, an analytical model of the storage system was devised. The stratification device (plate) makes this model innovative, because the storage system is heated at the bottom, with a concentrated solar collector. The channel located between the plate and the upper wall of the storage assembly allows the deposition of hot water at the top (see Figure 1).

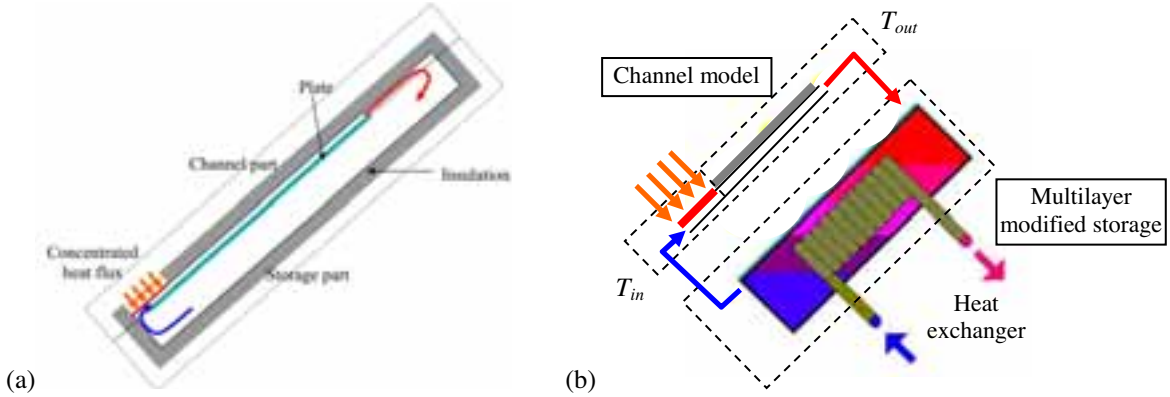

Fig. 1: (a) Diagram of the CFD model (b) Diagram of the analytical channel and the modified storage assembly

To model the new ICS system, an analytical model of the channel was coupled to a multilayer storage system model available in TRNSYS software (type 541 - TESS library). The latter was first modified to account for the boundary conditions imposed by the new ICS system (see Figure 1). The new model was compared to a numerical model (CFD type).

2. Governing equations and boundary conditions

2.1. Stratifier Channel

The equivalent electrical network model of the channel is shown in Figure 2. The channel can be divided into two zones: (i) the heating zone where the upper side has a fixed heat flux ($\dot{q}$), while the lower side allows a heat exchange with the bottom part of the storage system, and (ii) the cooling zone where the channel exchanges with both the environment and the storage assembly. The heat transfer within the channel is calculated using the temperature field obtained from the modified multilayer storage model.

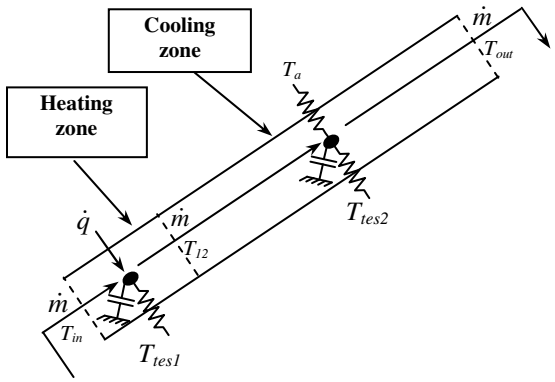

Fig. 2: Electrical network model of the channel.

The channel has the following dimensions: thickness e=0.003 m, height in the first part H_{ch1}=0.2 m and H_{ch2}=0.65 m in the second part. The channel height is smaller than the entire storage height in order to avoid blocking the mass flow rate when the heat flux is low. In this case, the buoyancy forces are calculated with the temperatures in the middle and the bottom parts of the storage unit (T_1 to T_7). The inlet temperature, T_{in}, is given by the bottom temperature in the storage unit T_1 from the first layer. T_{tes1} and T_{tes2} are the average temperatures between T_1 to T_2 and T_3 to T_7, respectively. T_a for the simulation cases is equal to 20°C.

Note that the inlet of the channel has a thermal diode such that when the channel temperature is lower than the storage temperature ($\dot{m}$=0), the hot zone becomes a heat accumulator.
The mass and heat balance equations in the channel are written as:

$$\Delta P_{in} + \Delta P_{chanel} + \Delta P_{out} = \Delta P_{tes} \rightarrow \frac{\dot{m}}{2}\left(\frac{\xi_{in}}{\rho_{in} A_{in}^2} + fr \frac{L_{ch}}{2e\overline{\rho}_{ch} A_{ch}^2} + \frac{\xi_{out}}{\rho_{out} A_{out}^2} \right) = g L_{ch} \cos(\Theta)(\overline{\rho}_{tes} - \overline{\rho}_{ch}) \quad \text{(eq.1)}$$

$$C_{ch1} \frac{dT_{ch1}}{dt} = \dot{q} \cdot A_{ch1} + \dot{m} c_{p_{in}} (T_{in} - T_{12}) + U_{ch1/tes1} \cdot A_{ch1} (T_{tes1} - T_{ch1}) \quad \text{(eq.2)}$$

$$C_{ch2} \frac{dT_{ch2}}{dt} = \dot{m} c_{p_{12}} (T_{12} - T_{out}) + U_{ch2/Ta} \cdot A_{ch2} (T_a - T_{ch2}) + U_{ch2/tes2} \cdot A_{ch2} (T_{tes2} - T_{ch2}) \quad \text{(eq.3)}$$

To calculate the friction factor (fr) and the mean convective heat transfer coefficient in the channel (h_{ch}), the correlations given by (Muzvchka et al. 2004; Muzychka and Yovanovich 2009) were used. These correlations are based on the section area of the channel for a noncircular duct. The friction factor fr is given by:

$$fr \cdot \mathrm{Re}_{\sqrt{A}} = \left[\left(\frac{3.44}{\sqrt{z^+}} \right)^2 + \left(\frac{12}{\sqrt{\varepsilon} \cdot (1+\varepsilon) \cdot \left[1 - \frac{192 \cdot \varepsilon}{\pi^5} \cdot \tanh\left(\frac{\pi}{2 \cdot \varepsilon} \right) \right]} \right)^2 \right]^{0.5} \quad \text{(eq.4)}$$

where $z^+ = W/((eW/2)^{0.5}\,\mathrm{Re}_{\sqrt{A}})$, the dimensionless position for hydrodynamically developing flow, ε is the aspect ratio e/W, and $\mathrm{Re}_{\sqrt{A}}$ the Reynolds number based on square root of flow area. The mean convective heat transfer coefficient in the channel (h_{ch}) is written as follows:

$$h_{ch} = Nu_{\sqrt{A}} \cdot \frac{k}{(e \cdot W)^{0.5}} \quad \text{(eq.5)}$$

$$Nu_{\sqrt{A}(Z^*)} = \left[\left(\frac{2 f(\mathrm{Pr})}{\sqrt{z^*}} \right)^{m^*} + \left(\left(\frac{3}{2} \cdot 0.501 \left(fr \frac{\mathrm{Re}_{\sqrt{A}}}{z^*} \right)^{1/3} \right)^5 + \left(3.86 \frac{fr\,\mathrm{Re}_{\sqrt{A}}}{8\sqrt{\pi}\varepsilon^{0.1}} \right)^5 \right)^{m^*/5} \right]^{1/m^*} \quad \text{(eq.6)}$$

where $z^* = (H/(eW)^{0.5})/(\mathrm{Re}_{\sqrt{A}}\,\mathrm{Pr})$ is the dimensionless position for thermally developing flow, $f(\mathrm{Pr}) = 0.886/(1+(1.909\,\mathrm{Pr}^{1/6})^{9/2})^{2/9}$, and $m^* = 2.27 + 1.65\,\mathrm{Pr}^{1/3}$.

The mean temperature in the channel 1 (T_{ch1}) is given by the average of T_{in} and T_{12}. To determine the energy balance in channel 2, its mean temperature (T_{ch2}) and the outlet temperature (T_{out}) can be calculated as follows:

$$T_{ch2} = \frac{T_{Wch} + (T_{Wch} - T_{12})}{(aH_{ch1})} \cdot (\exp(-aH_{ch1}) - 1) \quad \text{(eq.7)}$$

$$T_{out} = T_{Wch} - (T_{Wch} - T_{12}) \cdot \exp(-aH_{ch1}) \quad \text{(eq.8)}$$

where $a = (2W \cdot h_{ch2})/(\dot{m} \cdot c_{ch2})$ and T_{Wch} is the channel wall temperature, which is the average between the two internal wall temperatures.

2.2. Modified storage tank

For the storage component, we chose to modify the software model in TRNSYS (type 541 TESS library). The software version works with direct or indirect withdrawal in the storage tank (with or without an immersed heat exchanger), but not with both. The model's boundary conditions were modified to provide one flow inlet, one flow outlet, and an internal heat exchanger. This model presents the following advantages: (i) the storage tank is a rectangular box (here 1.3×1.5×0.1 m H×W×L), with different heat transfer coefficients on the top, side and lower surfaces; (ii) the storage assembly can work tilted and the buoyancy forces are taken into account in the calculation. In the comparison study between the CFD results and the new model, the modified type was considered to be a black box. The time step equal to 1 min was used in the simulation.

The storage unit is divided into ten temperature layers, where *N1* is the layer at the bottom and *N10* at the top. The global heat transfer coefficient around the storage is U=2W/m²K. In the modified case, the outlet flow is at the bottom, which is the inlet for channel 1 with $\dot{m}$ and T_{in} =T_1, and the inlet at the top, with $\dot{m}$ and T_{out} from channel 2. The inlet at the top (*N10*) was chosen because with the low velocity on the output of the channel it is possible to consider the inlet at the top.

In this paper, the details on how the model is solved will not be described, see references in (TRNSYS-TESS 2004).

2.3. CFD Model

The CFD results are based on a cavity with the following dimensions (Figure 3), where a Bousinesq approach and the shear stress transfer, SST-turbulence model from (ANSYS-Inc. 2009) are used, with a time step equal to 0.75 s. This CFD model was previously validated by experimental results.

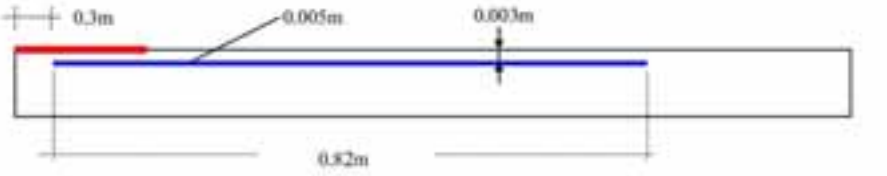

Fig. 3: Diagram of the storage and plate dimensions for the CFD model.

The following boundary conditions are applied in both models. The initial storage temperature is T_i=20°C and the ambient temperature T_i=T_a. The global heat transfer coefficient around the storage is U=2W/m²K. To compare the two models, the following boundary conditions were modified:

Table 1: Boundary conditions changed in the models for the respective cases

Cases	Slope angle (deg)	Heat flux (W/m²)
A30P18	30	1800
A30P36	30	3600
A45P18	45	1800
A45P36	45	3600

3. Results and discussion

The results over time of the following variables will be discussed: the temperature distribution, the average temperature, the cumulated energy in the storage system, the heat transfer through the plate, and the mass flow rate in the channel. Although the study of the time step is not discussed in this paper, the choice of 1 min was based on the results at the beginning of the simulation. The graph of the mass flow rate (Figure 7) illustrates the time step effect.

3.1. Average and temperature field

To show the temperature field's temporal evolution in the storage system, the temperatures T_1, T_3, T_5, T_7, and T_9 were chosen, where T_1 is at the bottom and T_9 at the top (Figure 4 and Figure 5). In all the cases studied, the temperature at the top (T_9) and at the bottom (T_1) was higher for the model at any time. Conversely, for T_7 the CFD model was always higher. In all cases, the major difference between the temperatures of the models was about 0.5°C.

The influence of the slope angle was low; the stratification in the storage unit changed very little between 30° and 45°, but a higher temperature can be observed in the 30° cases. Overall, the distribution and changes in the temperature in the model storage tank were satisfactory when compared with the CFD model.

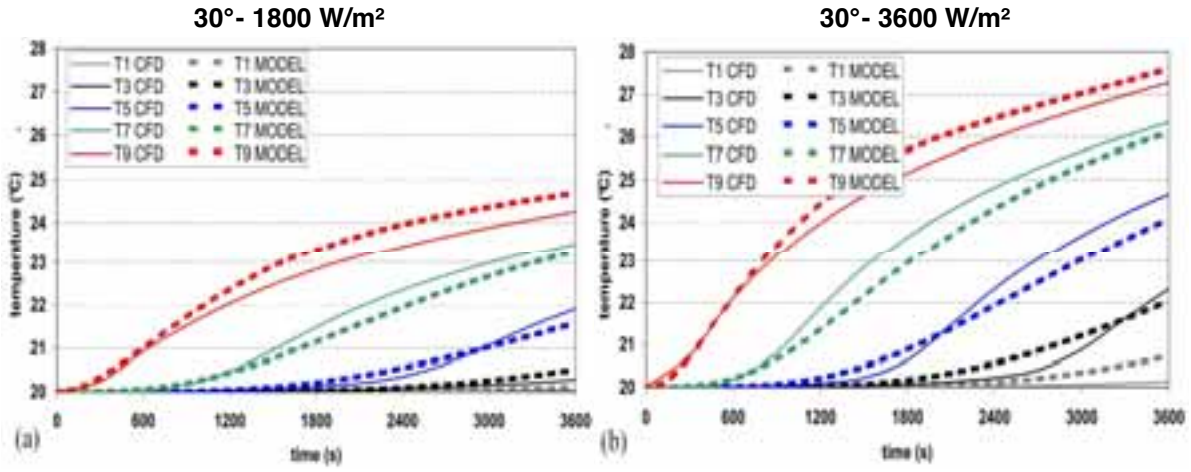

Fig. 4: Temperature field in the storage system for CFD and MODEL (a) A30P18; (b) A30P36.

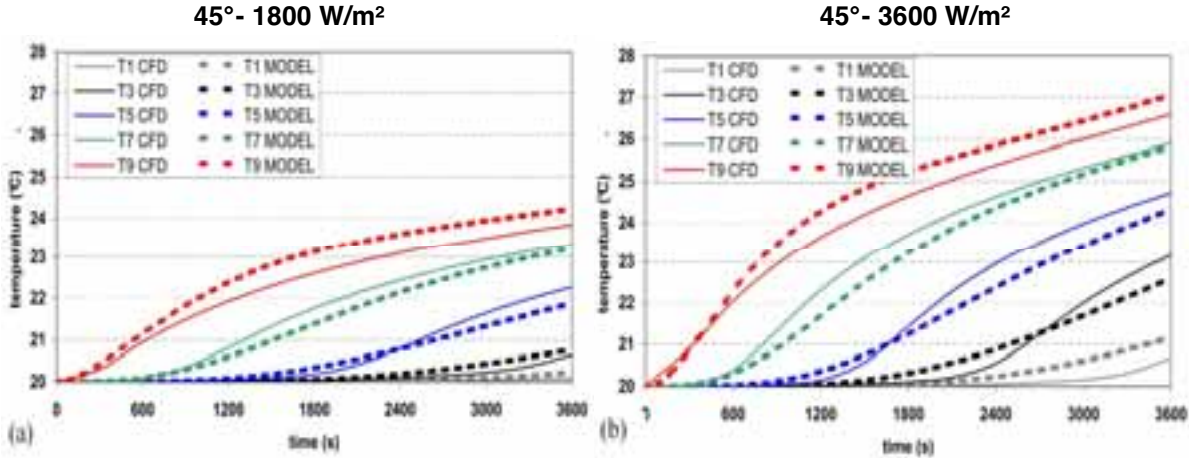

Fig. 5: Temperature field in the storage system for CFD and MODEL (a) A45P18; (b) A45P36.

Regarding the changes in average temperature (Figure 6), a substantial discrepancy appeared in the average temperature for t<1200 s. The average temperature change in these cases can be represented by a straight line, even if the CFD model has a slightly curved profile at its beginning and a higher mean temperature can be expected for the CFD model after 1 h. For A45P35, this change already appeared at t=3600 s with a 0.02°C increase for the model.

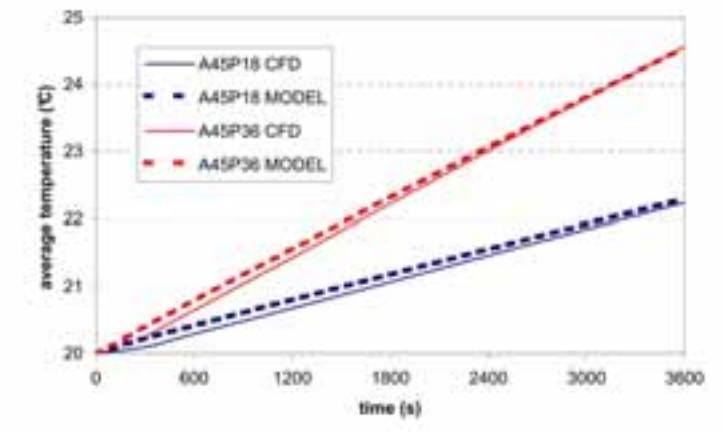

Fig. 6: Average temperature in the storage system for CFD and MODEL, A45P18 and A45P36.

3.2. Energy balance

To determine the energy balance from the models, the differences between models can be better quantified. Table 2 shows the cumulated energy for both models and the percentage variation at 1200 s, 2400 s, and 3600 s. In general, the discrepancy between the CFD and the model decreases with time. At t=1200 s, the difference reached approximately 19% for A45P36, until it inversed at t=3600 s for A30P36 and A45P36 with −0.16% and −0.54%, respectively.

Tab. 2: Cumulated energy for both models at t=1200s, t=2400s, and t=3600s.

CASE	CFD - Cumulated energy (kj)	MODEL - Cumulated energy (kj)	(MODEL-CFD)/ MODEL (%)
	t=1200s		
A30P18 (30° - 1800 W/m²)	543.00	624.05	12.99
A30P36 (30° - 3600 W/m²)	1153.50	1307.48	11.78
A450P18 (45° - 1800 W/m²)	551.16	683.14	19.32
A45P36 545° - 3600 W/m²°	1168.70	1327.06	11.93
	t=2400s		
A30P18	1184.10	1267.01	6.54
A30P36	2433.40	2504.01	2.82
A45P18	1192.26	1281.48	6.96
A45P36	2459.00	2526.19	2.66
	t=3600s		
A30P18	1819.00	1853.78	1.88
A30P36	3688.14	3682.23	−0.16
A45P18	1827.15	1870.62	2.32
A45P36	3727.17	3707.27	−0.54

As for the previous variables, the mass flow rate is higher for the model (Figure 7). This difference has its maximum in 0.0031 kg/s for A45P36 at t=3600 s and the minimum in 0.0009 kg/s, representing an error of about 8.5% and 3.2%, respectively. At the beginning of the new model simulation, a peak can be observed, resulting from the time step. Even with a lower time step, the mass flow rate is lower for the CFD model.

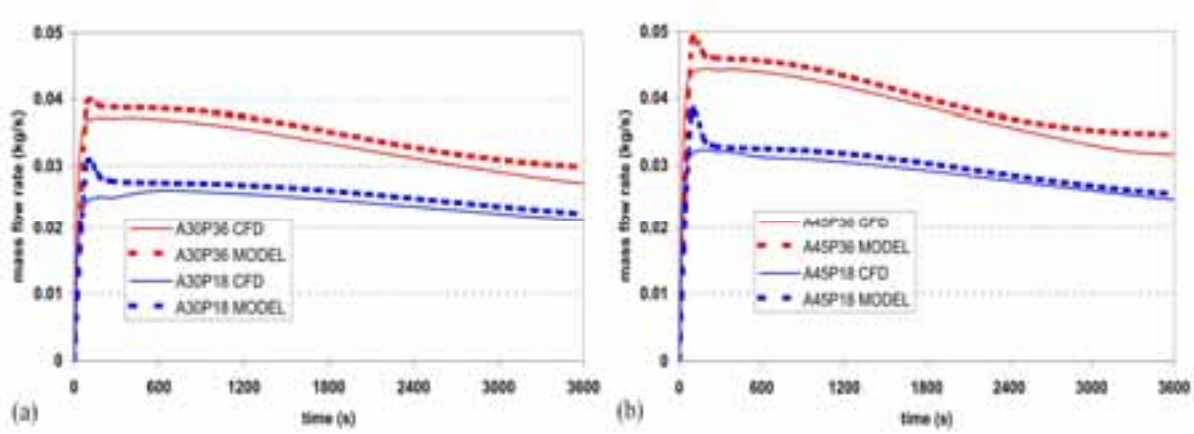

Fig. 7: Mass flow rate for CFD and MODEL (a) A30P36 and A30P18; (b) A45P36 and A45P18.

Concerning the heat flux between the channel and the storage system (Figure 8) before t=1200 s, the CFD heat flux is lower and increases slowly. This phase shift occurs because the CFD model takes into account the heat capacity of the plate. After this time, for the storage units heated with the 3600 W/m², the model heat flux is lower, and for the other storage units, heated with 1800 W/m², the CFD heat flux is slightly higher.

The other losses on the back and side surfaces are slightly lower for the CFD, approximately 2%. To explain the difference in cumulated energy, the temperature fields, and the mass flow rate, the heat flux between the channel and the environment must be analyzed (Figure 9). At t=300s the CFD model is about 75% higher, for all configurations and at t=3600 s this difference is about 80%.

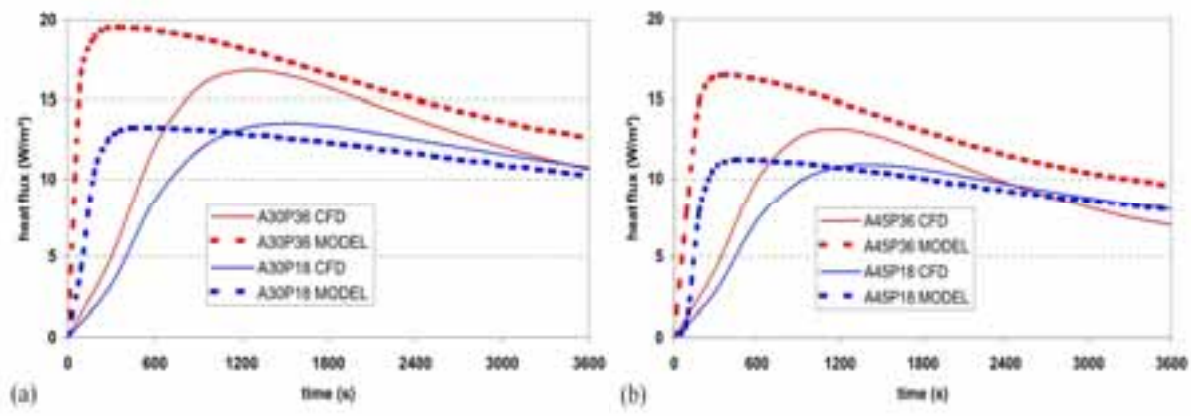

Fig. 8: Heat flux between channel and the modified storage unit for CFD and MODEL (a) A30P36 and A30P18; (b) A45P36 and A45P18.

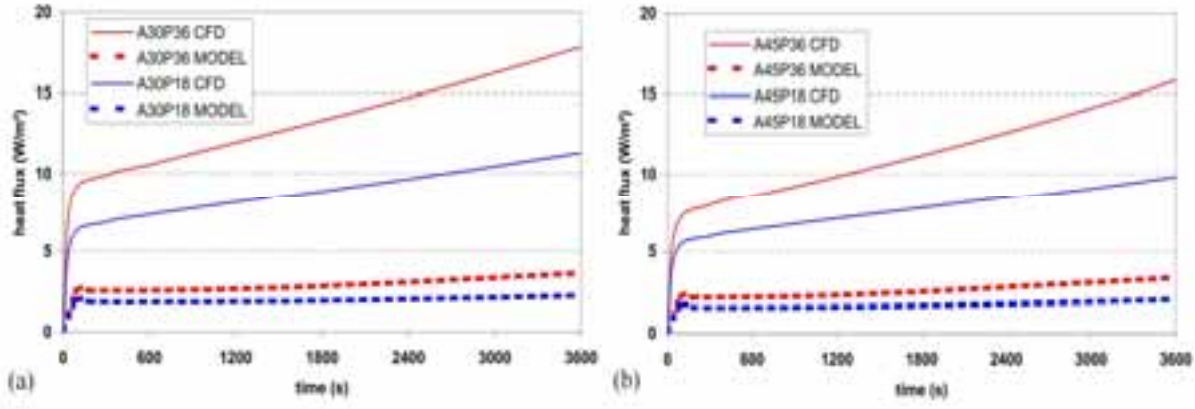

Fig. 9: Heat flux between channel and the ambient temperature for CFD and MODEL (a) A30P36 and A30P18; (b) A45P36 and A45P18.

This considerable difference in the heat flux exchange with the environment can explain the model's behavior. Because a lower heat flux with the environment means less loss, then a higher average and outlet temperature in channel 2 and higher buoyancy forces, hence a higher mass flow rate.

In a general view, the global model can be considered satisfactory. It should also be mentioned that the calculation time for the CFD model is about 9 h to simulate 1 h. With the global model, this simulation takes less than 1 s, so for the annual simulation, a calculation time of about 2 h can be expected with a 1-min time step.

4. Annual Simulation

During this study, four annual simulations were carried out, where the two heat exchangers for domestic hot water and two storage capacity systems were studied. The daily withdrawal used in these simulations is 0.083 kg/s at t=8 h and t=19 h for 20 min each (100 l in each withdrawal) where the inlet temperature in the heat exchanger is equal to 15°C. The weather data from Chambery, France, were used for the simulations. The new ICS has a 30° inclination angle.

3.2. Assembling with the thermal collector

The new model was assembled with a thermal collector, an evacuated solar tube, and an annual simulation was carried out. This thermal collector (evacuated tube type) exchanges the heat flux at the bottom of the new model, working as a solar radiation concentrator. The solar collector has a 2-m² surface collector and its efficiency is given by:

$$n = 0.75 - 2.5\left(\frac{Tm - Ta}{G}\right) - 0.007\left(\frac{(Tm - Ta)^2}{G}\right) \qquad \text{(eq.9)}$$

where *Tm* is the average temperature at the collector, *Ta* is the external temperature, and *G* is the total incident solar radiation.

3.2. Heat exchanger effect

To supply domestic hot water, the heat exchanger must be taken into account. For these preliminary simulations, a copper serpentine heat exchanger was chosen, 30 m long with an internal diameter of 0.025 m. This paper does not discuss heat exchanger optimization but only the distribution effect of the heat exchanger in the storage system. The results are given by a heat exchanger distributed uniformly throughout the height of the storage tank (HX1) and with a more concentrated heat exchanger on the top (HX2).

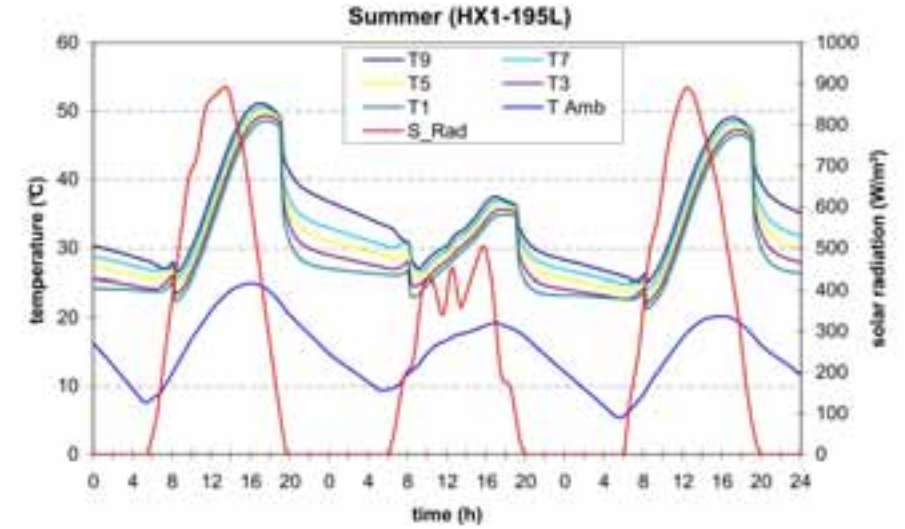

Fig. 10: Summer day's results of the annual simulation with HX1.

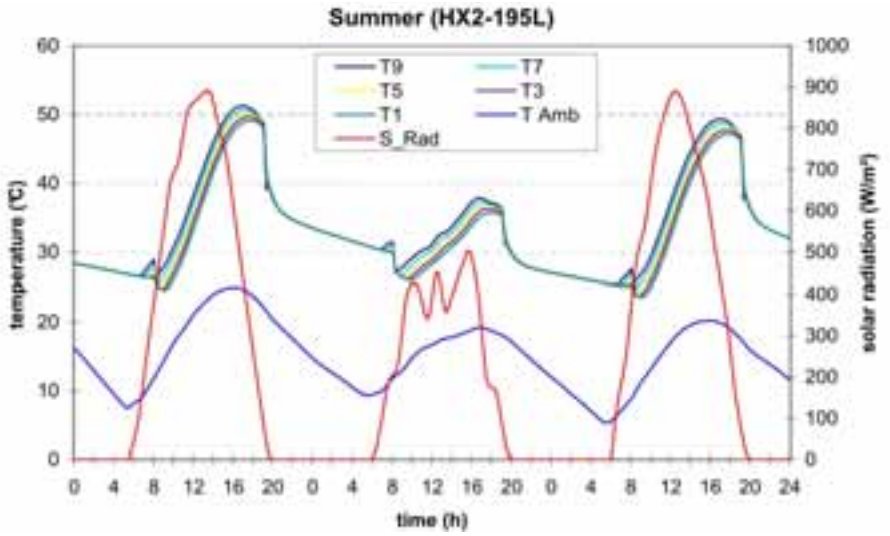

Fig. 11: Summer day's result of the annual simulation with HX2.

Figures 10 and 11 represent three summer days in the annual simulation. For HX1, an increase in the stratification after the withdrawal was observed; with the HX2, a uniform temperature was observed. In useful domestic hot water, the differences between the two heat exchangers are given in Table 3. For these examples, the effect of the heat exchanger distribution was not significant.

Tab 3: Outlet HX average temperature for summer, winter, and average year.

	Outlet HX average temperature (°C)	
CASE	HX1	HX2
Summer average - morning	25.3	25.8
Summer average - afternoon	40.4	39.8
Winter average - morning	17.3	18.2
Winter average - afternoon	24.8	25.6
Year average - morning	22.1	22.8
Year average - afternoon	34.1	34.1

3.2. The volume storage effect

In the previous simulations, the surface collector (m^2)/volume storage (m^3) ratio was equal to 10.25 (m^2/m^3). For the following simulations, a ratio of 12.82 (m^2/ m^3) was used, which results in a storage system of the following dimensions: 1.3×1.5×0.08 m with, respectively, *H*×*W*×*L* and a volume equal to 0.096 m^3.

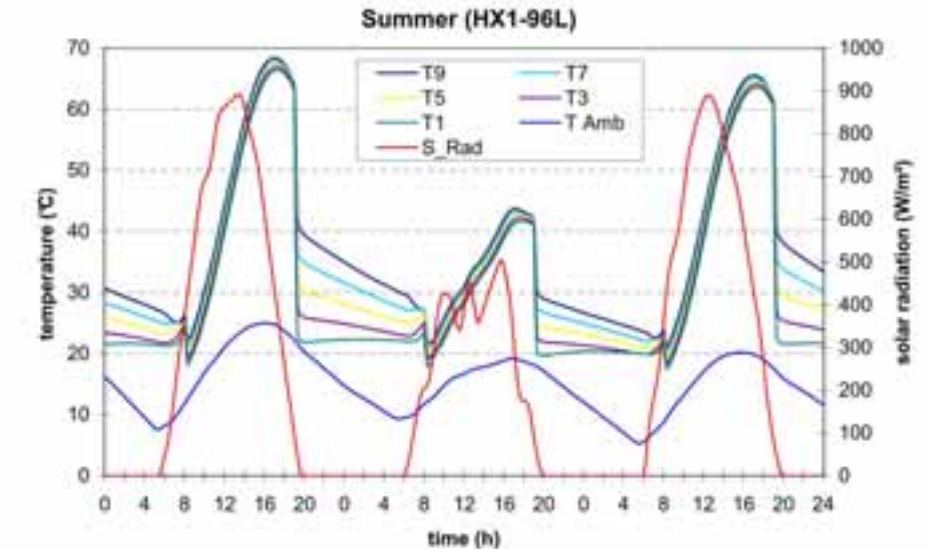

Fig. 11: Summer day's result of the annual simulation with HX1 and volume storage equal to 0.096 m^3.

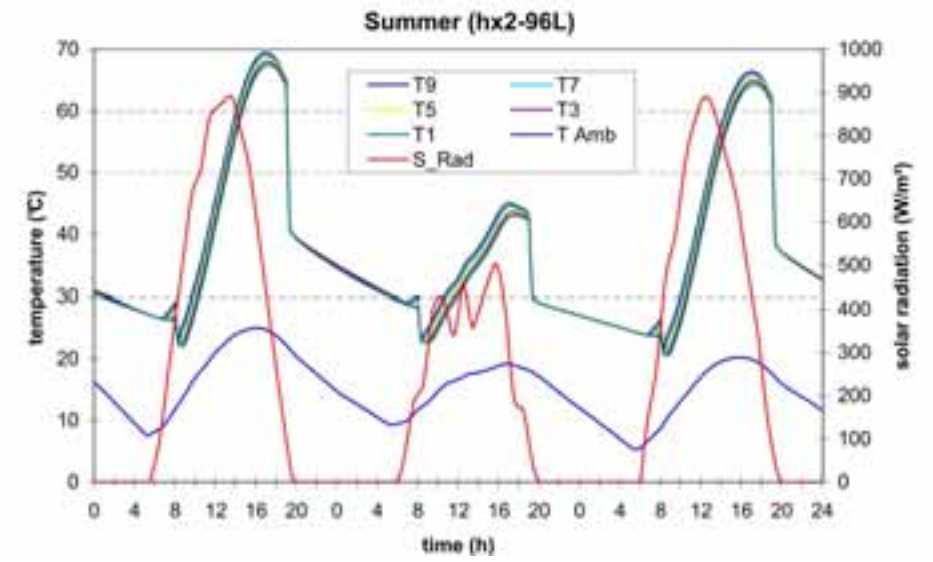

Fig. 11: Summer day's result of the annual simulation with HX2 and volume storage equal to 0.096 m^3.

Comparing these results with the configuration volume 0.195 m^3, a higher temperature was observed in the afternoon and a lower temperature in the morning. Moreover, the increase in the afternoon temperature was greater than the decrease in the morning temperature. As for the heat exchanger distribution, the HX1 had a better annual performance in the afternoon versus a better morning performance for the HX2.

Tab. 4: Outlet HX average temperature for summer, winter, and average year.

	Outlet HX average temperature (°C)	
CASE	HX1	HX2
Summer average - morning	21.9	23.6
Summer average - afternoon	43.9	44.1
Winter average - morning	15.5	16.4
Winter average - afternoon	26.4	26.4
Year average - morning	19.3	20.7
Year average - afternoon	36.9	37.0

In all configurations, the new ICS resisted freezing temperatures as Figure 12 shows for 3 winter days, for the HX2-0.096 m^3 example. Note that even with indirect withdrawal, in winter, the inlet water in the heat exchanger can increase the average temperature in the storage unit and avoid the risk of freezing. For the configurations simulated in this experiment, the risk of freezing was not relevant; the lowest temperature in all simulations was about 14°C for the HX2-0.096 m^3.

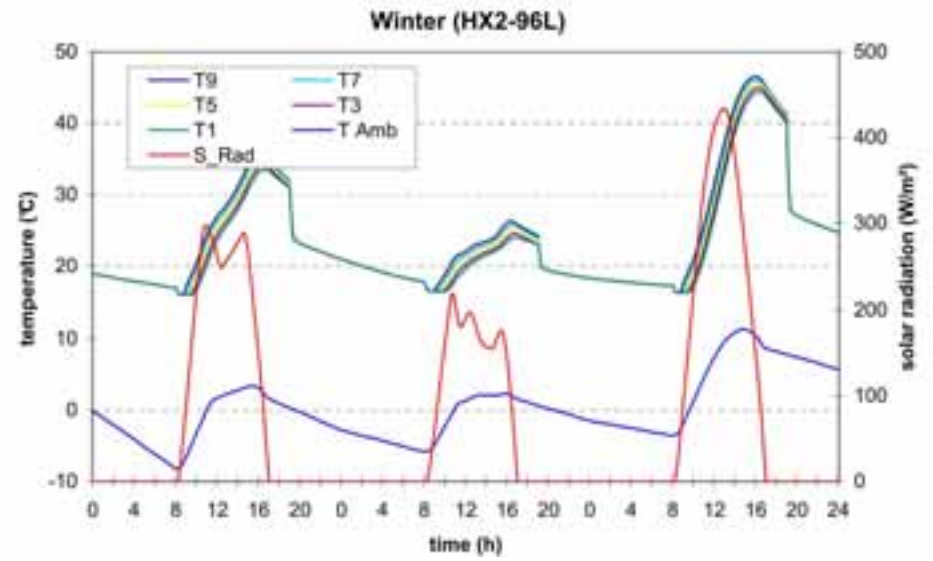

Fig. 11: Winter day's result of the annual simulation with HX2 and volume storage equal to 0.096 m^3.

5. Conclusions and perspectives

This paper has compared and validated a new ICS model using a numerical model (CFD type). The outcomes of this validation procedure show that: (i) in terms of accumulated energy, a discrepancy of −1 to 20% was observed between the new model predictions and the numerical results, and this difference was greater at the beginning of the simulation, (ii) in terms of temperature field and mass flow rate, the new model predicts higher values, and (iii) these discrepancies are caused by the low heat flux prediction between the channel and the environment, because a lower heat flux with the environment means less loss in channel 2, then a higher average and outlet temperature, higher buoyancy forces, hence a higher mass flow rate.

In the annual simulation, the storage was assembled with an evacuated tube collector. The distribution of the heat exchanger within the storage tank was analyzed and the two volume storage systems were simulated. The heat exchanger distribution was not significant for the two HXs studied. Reducing the storage volume, the outlet temperatures in the HX are higher in the afternoon and lower in the morning, but in an overall view, efficiency is greater in the smaller volume. During all the simulations, the risk of freezing was null for all configurations of the new model.

An optimization study of the heat exchanger is planned with other withdrawal profiles. In order to adapt the ICS system for distinct regions in France, the collector surface/volume storage ratio will be investigated to optimize this variable. After modeling the new ICS unit, a prototype will be made and tested in real conditions.

6. References

ANSYS-Inc. (2009). ANSYS-CFX 12 User guide

Muzvchka, S. Y, Yovanovich and N. M (2004). Laminar forced convection heat transfer in the combined entry region of non-circular ducts. New York, NY, ETATS-UNIS, American Society of Mechanical Engineers.

Muzychka, Y. S. and M. M. Yovanovich (2009). "Pressure Drop in Laminar Developing Flow in Noncircular Ducts: A Scaling and Modeling Approach." Journal of Fluids Engineering 131(11): 111105.

TRNSYS-TESS (2004). TRNSYS-TRaNsient SYstem Simulation program. Volume A2 - TESS Libraries - Type541 - User Manual.